Rare Metal Materials and Engineering
Volume 52, Issue 3, March 2023
Available online at www.rmme.ac.cn

Science Press

Cite this article as: Jiang Wentao, Wang Ye, Jiang Bo, et al. Microstructure and Mechanical Properties of $Al_{0.5}Nb_{1.5}TiV_2Zr_{0.5}$ Refractory High Entropy Alloy[J]. Rare Metal Materials and Engineering, 2023, 52(03): 846-851.

ARTICLE

Microstructure and Mechanical Properties of $Al_{0.5}Nb_{1.5}TiV_2Zr_{0.5}$ Refractory High Entropy Alloy

Jiang Wentao[1], Wang Ye[1], Jiang Bo[1], Wang Xiaohong[2], Ma Tengfei[2], Zhu Dongdong[2]

[1] School of Materials Science and Chemical Engineering, Harbin University of Science and Technology, Harbin 150040, China; [2] Key Laboratory of Air-Driven Equipment Technology of Zhejiang Province, Quzhou University, Quzhou 324000, China

Abstract: The $Al_{0.5}Nb_{1.5}TiV_2Zr_{0.5}$ high entropy alloy was prepared by vacuum arc melting, and its microstructure, density, and mechanical properties were investigated. Results show that $Al_{0.5}Nb_{1.5}TiV_2Zr_{0.5}$ alloy consists of 90.6vol% body-centered cubic phase and 9.4vol% C14-Laves secondary phase. The matrix phase of the alloy is rich in Ti and V, and the secondary phase is rich in Al and Zr. The alloy has a low density of 6284 kg/m^3 and Vickers hardness of 5197.9 MPa. The yield strength of alloy is decreased with increasing the temperature: it decreases from 1082.9 MPa at room temperature to 645.0 MPa at 1073 K. The compressive strain decreases from 27.20% at room temperature to 14.94% at 873 K, which is related to the decrease in atomic interaction force when the temperature rises. At 1073 K, the compressive strain of alloy exceeds 50%, indicating the good plasticity without fracture. The results of compression tests show that the ductile-brittle transition temperature ranges from 873 K to 1073 K.

Key words: $Al_{0.5}Nb_{1.5}TiV_2Zr_{0.5}$; high entropy alloy; microstructure; hardness; compressive property

Composition adjustment can modify the microstructure of traditional alloys, thereby leading to enhancement in alloy properties. However, the excessive addition of alloying elements will inevitably result in the brittleness of alloy, thus greatly restricting the development and innovation of traditional alloys. Therefore, high entropy alloy (HEA), which breaks the traditional alloying design and promotes the alloy properties, has been proposed and researched in the past decade[1–2]. Due to its excellent properties, HEA has attracted extensive attention. HEAs are usually composed of five or more alloying elements with equal or nearly equal atomic ratios[3–5].

High temperature materials are highly required in aerospace field, and the Ni-based alloys have been widely used due to their excellent environment resistance and mechanical properties at high temperatures[6–8]. Although Ni-based alloys have an optimal combination of properties at high temperatures of about 1000 °C, their application at even higher operating temperatures is restricted because of their relatively low melting temperatures. Thus, it is of importance to develop the novel high temperature materials. Considering the advantages of HEAs and the wide application of refractory alloys, the refractory high entropy alloys (RHEAs) show great potential in service at high temperatures. The excellent high temperature strength, good phase stability, and fine high temperature oxidation resistance of RHEAs have been extensively researched[9–14]. Zeng et al[14] developed the NbMoTaW and VNbMoTaW RHEAs with excellent properties at high temperatures: the yield strength was more than 400 MPa at 1600 °C. Based on the lightweight design concept of HEAs, the novel lightweight RHEAs are developed[15–20]. Lightweight RHEAs have higher specific strength and hardness than the traditional lightweight alloys do, and their density is much lower than that of common RHEAs, such as NbMoTaW alloy. The density of Ti_2ZrVNb alloy is only 6.12 g/cm^3, and its specific strength can reach about 180 kPa·m^3·kg^{-1}, which is better than those of other HEAs at room temperature[19]. The $AlNbTiVZr_{0.5}$ alloy with good plasticity has density of 5.63 g/cm^3, specific strength of 254 kPa·m^3·kg^{-1} at room temperature, and specific strength of 121 kPa·m^3·kg^{-1} at 800 °C[16]. Nevertheless, the lightweight RHEAs are rarely reported. The research on the structure and

Received date: May 16, 2022
Foundation item: National Natural Science Foundation of China (52171113)
Corresponding author: Wang Ye, Ph. D., School of Materials Science and Chemical Engineering, Harbin University of Science and Technology, Harbin 150040, P. R. China, E-mail: wangye1984@hrbust.edu.cn

mechanical properties of lightweight RHEAs can provide reference and technical support for the production and manufacture of lightweight alloys, thereby promoting their application.

In this research, the $Al_{0.5}Nb_{1.5}TiV_2Zr_{0.5}$ RHEA was investigated, and its microstructure and mechanical properties at room temperature and high temperature were analyzed.

1 Experiment

Al, Nb, Ti, V, and Zr powders with high purity (≥99.9wt%) were mixed with the molar ratio of 0.5 : 1.5 : 1.0 : 2.0 : 0.5. Vacuum arc melting was conducted in the water-cooled copper crucible in argon atmosphere. The alloy ingot was melted at least 5 times to ensure the homogeneousness of components.

The phase composition and microstructure of the alloy were studied by X-ray diffraction (XRD) and scanning electron microscope (SEM). XRD analysis was performed by D8 Advance diffractometer with Cu-Kα radiation. Hitachi SU8010 SEM coupled with energy dispersive spectrometer (EDS) was used for chemical composition analysis. The content of different phases observed by SEM at back-scattered electron (BSE) mode was measured by ImageJ software. Different components of specimens were analyzed 3–5 times to determine the element distribution.

The alloy density was measured by Archimedes method, and the average value of five measurements was used for analysis. The Shimadzu DUH-211S hardness tester was used to measure the Vickers hardness of the smooth alloy surface with a load of 1000 mN and keeping for 20 s. Eleven points on the specimen were selected for hardness measurement. The MTS 370 electronic universal testing machine was used to compress the specimens with size of *Φ*4.0 mm×6.0 mm at different temperatures (298, 673, 873, and 1073 K), and the initial strain rate was 1×10^{-3} s^{-1}. Before the compression test, the specimen surface was polished to reduce the impact of scratches on stress. The fracture morphologies of the $Al_{0.5}Nb_{1.5}TiV_2Zr_{0.5}$ alloy after compression tests were observed by Hitachi SU8010 SEM.

2 Results and Discussion

2.1 XRD analysis and microstructure characteristics

Fig. 1 shows XRD pattern of the as-cast $Al_{0.5}Nb_{1.5}TiV_2Zr_{0.5}$ RHEA. It can be seen that the $Al_{0.5}Nb_{1.5}TiV_2Zr_{0.5}$ RHEA consists of body-centered cubic (bcc) matrix phase and C14-Laves secondary phase. The lattice constant of bcc phase is determined as 0.327 nm, according to Bragg ' s law. The mixing theoretical lattice constant (a_{mix}) of $Al_{0.5}Nb_{1.5}TiV_2Zr_{0.5}$ RHEA can be estimated by Eq.(1) [21], as follows:

$$a_{mix} = \sum_{i=1}^{n} c_i a_i \quad (1)$$

where c_i is the content of element i in $Al_{0.5}Nb_{1.5}TiV_2Zr_{0.5}$ RHEA; a_i is the lattice constant of element i in $Al_{0.5}Nb_{1.5}TiV_2Zr_{0.5}$ RHEA; n is the total number of elements. As a result, a_{mix} =0.323 nm, which is similar to the experiment value, indicating that the $Al_{0.5}Nb_{1.5}TiV_2Zr_{0.5}$ RHEA basically obeys the mixing principle.

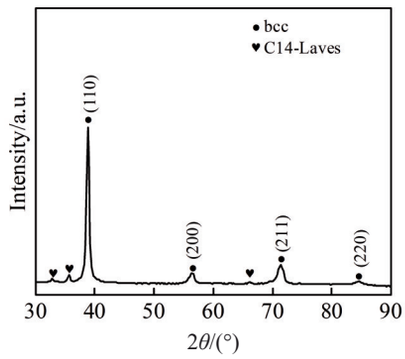

Fig.1 XRD pattern of as-cast $Al_{0.5}Nb_{1.5}TiV_2Zr_{0.5}$ RHEA

Fig. 2 shows SEM-BSE image of the microstructure of $Al_{0.5}Nb_{1.5}TiV_2Zr_{0.5}$ RHEA, confirming that this alloy consists of two structures. $Al_{0.5}Nb_{1.5}TiV_2Zr_{0.5}$ RHEA is dominated by the dark gray matrix phase (bcc phase) of 90.6vol%, and the light gray area of C14-Laves secondary phase accounts for 9.4vol% . The secondary phase is mainly distributed at the grain boundary of bcc phase. EDS results show that the chemical composition of bcc phase is similar to that of RHEA. Fig.2b–2f demonstrate that the bcc phase in $Al_{0.5}Nb_{1.5}TiV_2Zr_{0.5}$ alloy is rich in Ti and V, and the C14-Laves phase is rich in Al and Zr. Nb element is evenly distributed in bcc matrix phase and C14-Laves secondary phase, but Nb content in the C14-Laves secondary phase is slightly richer than that in the matrix phase.

2.2 Density and hardness of $Al_{0.5}Nb_{1.5}TiV_2Zr_{0.5}$ RHEA

The density of $Al_{0.5}Nb_{1.5}TiV_2Zr_{0.5}$ RHEA is 6284 kg/m^3, and the theoretical density of $Al_{0.5}Nb_{1.5}TiV_2Zr_{0.5}$ RHEA can be calculated by Eq.(2) [2], as follows:

$$\rho_{mix} = \frac{\sum_{i=1}^{n} c_i A_i}{\sum_{i=1}^{n} c_i A_i / \rho_i} \quad (2)$$

where A_i represents the atomic mass of i element, and ρ_i represents the density of i element. The theoretical density of $Al_{0.5}Nb_{1.5}TiV_2Zr_{0.5}$ alloy is calculated as 6280 kg/m^3, which is very close to the measured value, indicating that the elements of $Al_{0.5}Nb_{1.5}TiV_2Zr_{0.5}$ RHEA are completely melted during the melting process and their diffusion is relatively uniform.

Fig. 3 shows SEM morphology of the points for hardness measurement of $Al_{0.5}Nb_{1.5}TiV_2Zr_{0.5}$ alloy. Considering that the alloy is composed of bcc solid solution matrix phase and hard brittle C14-Laves secondary phase and the C14-Laves phase is mainly distributed at the grain boundary of bcc matrix phase in the elongated morphology, the hardness test points are distributed away from the C14-Laves phase to ensure the experiment accuracy. The Vickers hardness of $Al_{0.5}Nb_{1.5}TiV_2Zr_{0.5}$ RHEA is 5197.9 MPa.

2.3 Compressive properties

Fig. 4 shows the engineering stress-engineering strain curves of $Al_{0.5}Nb_{1.5}TiV_2Zr_{0.5}$ RHEA at 298 (room temperature), 673, 873, and 1073 K. The yield strength σ_{ys}, peak stress σ_p, and compressive strain ε of the $Al_{0.5}Nb_{1.5}TiV_2Zr_{0.5}$ RHEA at

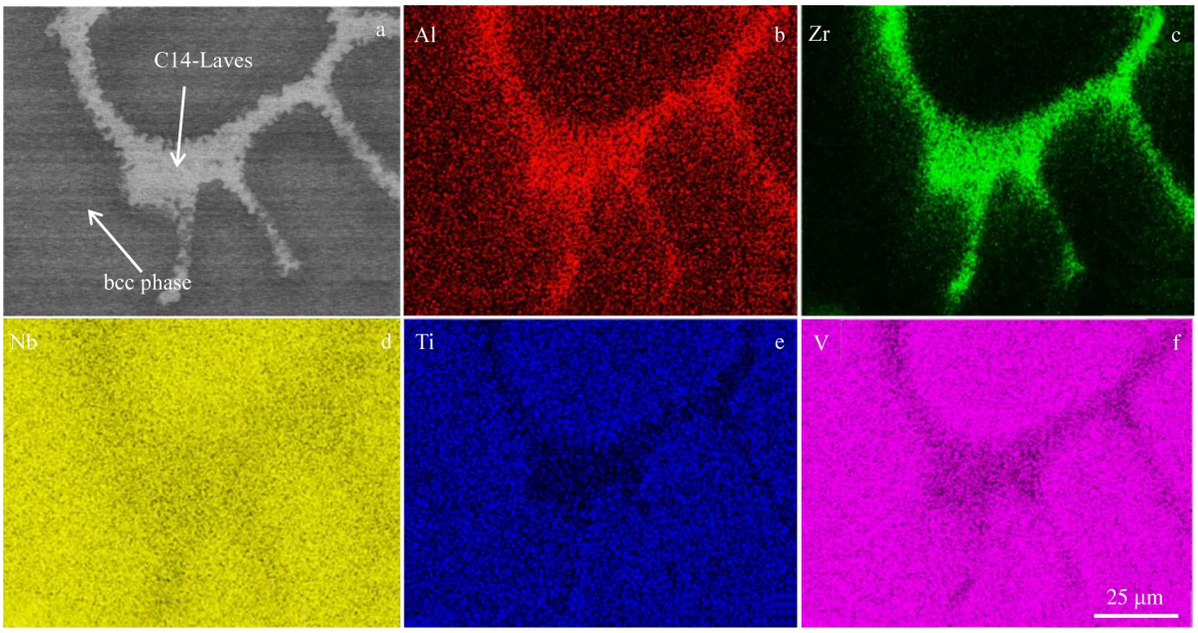

Fig.2 SEM-BSE image (a) and corresponding EDS element distributions of Al (b), Zr (c), Nb (d), Ti (e), and V (f) in $Al_{0.5}Nb_{1.5}TiV_2Zr_{0.5}$ RHEA

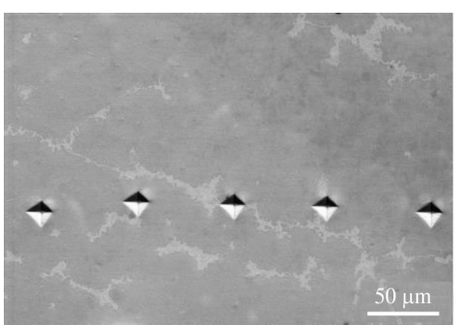

Fig.3 SEM morphology of Vickers hardness measurement points on $Al_{0.5}Nb_{1.5}TiV_2Zr_{0.5}$ RHEA

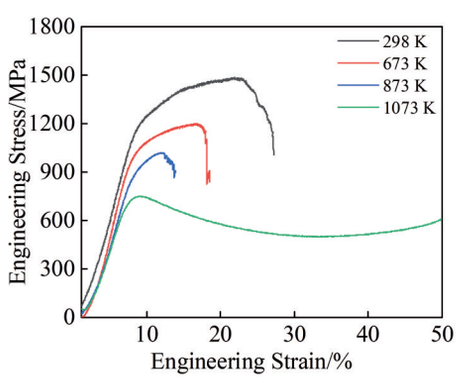

Fig.4 Engineering stress-engineering strain curves of $Al_{0.5}Nb_{1.5}TiV_2Zr_{0.5}$ RHEA at different temperatures

different temperatures are shown in Table 1. At 298, 673, 873, and 1073 K, the compressive yield strength of $Al_{0.5}Nb_{1.5}TiV_2Zr_{0.5}$ RHEA is 1082.9, 858.4, 772.3, and 645.0 MPa, respectively. With increasing the temperature, the yield strength of $Al_{0.5}Nb_{1.5}TiV_2Zr_{0.5}$ RHEA is gradually decreased to 645 MPa at

Table 1 Compressive yield strength (σ_{ys}), peak stress (σ_p), and compressive strain (ε) of $Al_{0.5}Nb_{1.5}TiV_2Zr_{0.5}$ RHEA at different temperatures

Temperature/K	Yield strength, σ_{ys}/MPa	Peak stress, σ_p/MPa	Compressive strain, ε/%
298	1082.9	1485.0	27.20
673	858.4	1199.0	18.55
873	772.3	1018.6	14.94
1073	645.0	750.3	>50

1073 K, the dynamic recovery of dislocation is increased, thus reducing the dislocation activity, and the formation rate of dislocation is decreased under the action of external stress[22–23]. In addition, at higher deformation temperatures, the preferred orientation and strength of the alloy are weakened by dynamic recrystallization[23], the resistance against dislocation movement is reduced, and the pinning effect of defects on dislocation is weakened. As a result, the compressive strength of the $Al_{0.5}Nb_{1.5}TiV_2Zr_{0.5}$ RHEA is decreased with increasing the temperature. At 298, 673, and 873 K, the strain corresponding to peak stress is 27.20%, 18.55% and 14.94%, respectively. With increasing the temperature, the strain corresponding to peak stress is decreased to 14.94% at 873 K. The decrease in plasticity of $Al_{0.5}Nb_{1.5}TiV_2Zr_{0.5}$ RHEA may be caused by the decrease in interatomic action force, which results from the increased temperature. Thus, the alloy is at an unstable or metastable state, leading to the decrease in plasticity of alloy. However, at 1073 K, the alloy is softened after reaching the peak stress. As a result, the strain of alloy exceeds 50%, and the ductile-brittle transition temperature of $Al_{0.5}Nb_{1.5}TiV_2Zr_{0.5}$ RHEA is 873 – 1073 K.

SEM fracture morphologies of the $Al_{0.5}Nb_{1.5}TiV_2Zr_{0.5}$ RHEA after compression tests at different temperatures are shown in Fig. 5. The compressive fracture of $Al_{0.5}Nb_{1.5}TiV_2Zr_{0.5}$ RHEA has obvious river patterns and tearing edges, suggesting the brittle fracture. With increasing the temperature, the fracture morphologies become smooth. Since the secondary phase with high hardness and high melting point has poor deformation capacity[24–26], the plasticity of $Al_{0.5}Nb_{1.5}TiV_2Zr_{0.5}$ RHEA is decreased with increasing the temperature during compression. Obvious cracks can be observed at the compressive fracture at 673 K, which may be the main reason for the reduction in compressive strain of the $Al_{0.5}Nb_{1.5}TiV_2Zr_{0.5}$ RHEA. However, the $Al_{0.5}Nb_{1.5}TiV_2Zr_{0.5}$ alloy does not fracture when the temperature exceeds the ductile-brittle transition temperature. The specimen was cut along the external stress direction and polished after compression test, and the specimen microstructure is shown in Fig. 5d. The typical coral-like dendritic structure can be observed. The light gray C14-Laves secondary phase is evenly distributed among the dendrites in a network form. It can also be observed that the microstructure of the $Al_{0.5}Nb_{1.5}TiV_2Zr_{0.5}$ RHEA becomes more compact under the external stress. The estimated content of bcc solid solution matrix phase is 81.5vol% , and that of the C14-Laves phase is 18.5vol% , which is about twice larger than the content of the secondary phase before compression.

The excellent mechanical properties of $Al_{0.5}Nb_{1.5}TiV_2Zr_{0.5}$ RHEA are attributed to the stable alloy structure, severe lattice distortion effect, and strengthening effect of C14-Laves phase. The valence electron concentration (VEC) can characterize the stability of alloy structure[27–28]. When VEC is greater than 8.0, it is easier to form stable face-centered cubic (fcc) phase; when VEC is 6.87–8.0, it is easier to form mixed fcc and bcc structure; when VEC is less than 6.87, it is easier to form bcc structure. VEC of $Al_{0.5}Nb_{1.5}TiV_2Zr_{0.5}$ RHEA is 4.55, indicating that a stable bcc structure is formed in $Al_{0.5}Nb_{1.5}TiV_2Zr_{0.5}$ RHEA. Besides, because the atomic radii of the principle alloying elements are different, particularly the large difference exists between Zr and V atomic radii, serious lattice distortion effect occurs, thus leading to the significant solid solution strengthening effect[2]. In addition, the binary mixture enthalpy formed by Al and Zr is −44 kJ/mol[16], suggesting the easy formation of stable hard brittle intermetallic compound phase. The C14-Laves phase of $Al_{0.5}Nb_{1.5}TiV_2Zr_{0.5}$ alloy is rich in Al and Zr, and a trace of C14-Laves phase is dispersed around the matrix phase in a network shape, indicating that the deformation mechanism of the alloy is mainly controlled by the C14-Laves phase, and the content of soft bcc solid solution phase does not affect the alloy strength[29]. Under continuous external stress, the soft phase is compressed to provide deformation capability, while the hard brittle C14-Laves phase hinders the dislocation movement to provide strength[30]. Therefore, the presence of C14-Laves phase with a certain content contributes to the excellent mechanical properties of $Al_{0.5}Nb_{1.5}TiV_2Zr_{0.5}$ RHEA, and the strengthening mechanism is the secondary phase strengthening.

Fig. 6 shows the relationships of specific yield strength of HEAs or RHEAs with the compressive strain and temperature[31–37]. The specific yield strength is defined as the ratio of strength to density. It can be seen that the alloys with higher specific yield strength at room temperature are generally more brittle, which may be related to the content of the hard brittle secondary phase in the alloy. In addition, it is obvious that the specific yield strength of the alloys is decreased gradually with increasing the temperature to 1073 K. As RHEA, the presence of a moderate content of Al/Zr-rich

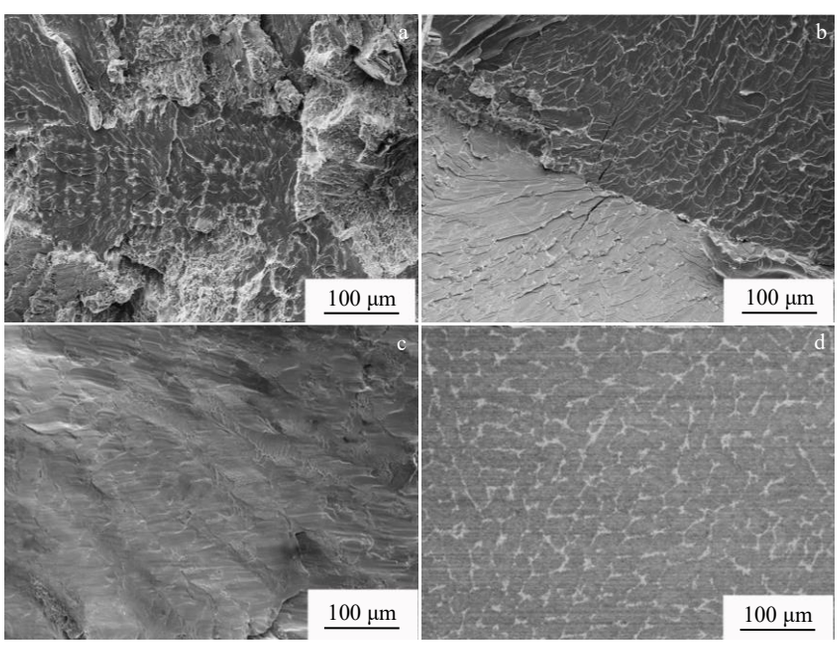

Fig.5 SEM compressive fracture morphologies of $Al_{0.5}Nb_{1.5}TiV_2Zr_{0.5}$ RHEA at 298 K (a), 673 K (b), and 873 K (c); SEM cross-section microstructure of $Al_{0.5}Nb_{1.5}TiV_2Zr_{0.5}$ RHEA at 1073 K (d)

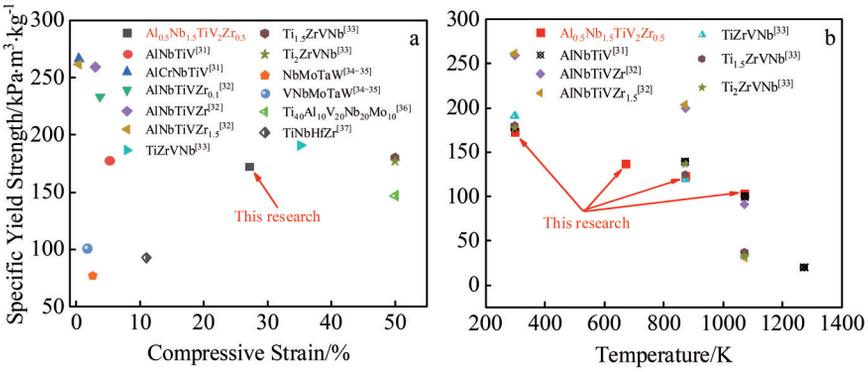

Fig.6 Specific yield strength of different HEAs/RHEAs at room temperature (a); relationships between specific yield strength and temperature of different HEAs/RHEAs (b)

intermetallic compound phase leads to the high strength of alloys at elevated temperatures. As a lightweight HEA, the specific yield strength of the alloy is varied gently with temperature due to its low density. It is observed from Fig.6b that the specific yield strength of some alloys is relatively high at room temperature, but it is decreased significantly with increasing the temperature. For the Al-Nb-Ti-V-Zr RHEAs with intermetallic compound phase of high melting point, the strength of alloy is commonly higher than that of the single bcc phase at high temperatures, and the content of intermetallic compound phase can also affect the alloy strength. In addition, the binding ability of the matrix to the secondary phase also plays a crucial role. Although some alloys have higher specific yield strengths than $Al_{0.5}Nb_{1.5}TiV_2Zr_{0.5}$ RHEA does at room temperature, the specific yield strength of $Al_{0.5}Nb_{1.5}TiV_2Zr_{0.5}$ RHEA is decreased gently with increasing the temperature, and the advantages of specific yield strength becomes more obvious at high temperatures than those of other RHEAs do.

3 Conclusions

1) The matrix phase of $Al_{0.5}Nb_{1.5}TiV_2Zr_{0.5}$ refractory high entropy alloy (RHEA) is the body-centered cubic (bcc) structure with lattice parameter of 0.323 nm. The content of bcc phase and C14-Laves phase is 90.6vol% and 9.4vol%, respectively. The bcc phase is rich in Ti and V, and the C14-Laves phase is rich in Al and Zr.

2) The density of $Al_{0.5}Nb_{1.5}TiV_2Zr_{0.5}$ RHEA is 6284 kg/m^3, which is approximately equal to the theoretical density. The Vickers hardness of $Al_{0.5}Nb_{1.5}TiV_2Zr_{0.5}$ RHEA is 5197.9 MPa.

3) Both the strength and plasticity of $Al_{0.5}Nb_{1.5}TiV_2Zr_{0.5}$ RHEA are decreased with increasing the compression temperature. At 298, 673, 873, and 1073 K, the compressive yield strength is 1082.9, 858.4, 772.3, and 645.0 MPa, respectively. At 298, 673, and 873 K, the strain corresponding to peak stress is 27.20%, 18.55% and 14.94%, respectively. But at 1073 K, the strain exceeds 50% and the alloy does not fracture.

4) The excellent mechanical properties of $Al_{0.5}Nb_{1.5}TiV_2Zr_{0.5}$ RHEA can be attributed to the stable alloy structure, severe lattice distortion effect, and strengthening effect of C14-Laves phase.

References

1 Yeh J W, Chen S K, Lin S J *et al. Advanced Engineering Materials*[J], 2004, 6(5): 299
2 Yeh J W. *Annales de Chimie Science des Materiaux*[J], 2006, 31(6): 633
3 Shi Y Z, Yang B, Xie X *et al. Corrosion Science*[J], 2017, 119: 33
4 Lee C P, Chang C C, Chen Y Y *et al. Corrosion Science*[J], 2008, 50(7): 2053
5 Chuang M H, Tsai M H, Wang W R *et al. Acta Materialia*[J], 2011, 59: 6308
6 Tsai Y L, Wang S F, Bor H Y *et al. Materials Science and Engineering A*[J], 2013, 571: 155
7 Wang X Y, Wang J J, Zhang C J *et al. Rare Metals*[J], 2021, 40(10): 2892
8 Li D S, Chen G, Li D *et al. Rare Metals*[J], 2021, 40(11): 3235
9 Li Yanchao, Li Laiping, Gao Xuanqiao *et al. Rare Metal Materials and Engineering*[J], 2020, 49(12): 4365 (in Chinese)
10 Wu Y D, Cai Y H, Wang T *et al. Materials Letters*[J], 2014, 130: 277
11 Wang Ruixin, Tang Yu, Li Yongyan *et al. Rare Metal Materials and Engineering*[J], 2020, 49(7): 2417 (in Chinese)
12 Wang F L, Balbus G H, Xu S Z *et al. Science*[J], 2020, 370(6512): 95
13 Jia Y Z, Hou Y Q, Wang P F *et al. Rare Metal Materials and Engineering*[J], 2022, 51(8): 2822
14 Zeng S, Zhou Y K, Li H *et al. Journal of Materials Science & Technology*[J], 2022, 130: 64
15 Senkov O N, Senkova S V, Miraclea D B *et al. Materials Science and Engineering A*[J], 2013, 565: 51
16 Stepanov N D, Yurchenko N Y, Sokolovsky V S *et al. Materials Letters*[J], 2015, 161: 136
17 Tan X R, Zhao R F, Bo R *et al. Materials Science and Technology*[J], 2016, 32(15): 1582

18 Zhao Haichao, Qiao Yulin, Liang Xiubing *et al*. *Rare Metal Materials and Engineering*[J], 2020, 49(4): 1457 (in Chinese)
19 Jiang W T, Wang Y, Wang X H *et al*. *Materials Science and Engineering A*[J], 2023, 865: 144 628
20 Li Gang, Wen Ying, Yu Zhongmin *et al*. *Rare Metal Materials and Engineering*[J], 2022, 51(5): 1681 (in Chinese)
21 Lin C M, Juan C C, Chang C H *et al*. *Journal of Alloys and Compounds*[J], 2015, 624: 100
22 Liu Ping, Chen Zhongjia. *Journal of Hefei University of Technology*[J], 2011, 34(3): 341 (in Chinese)
23 Wang B J, Wang Q Q, Lu N *et al*. *Journal of Materials Science & Technology*[J], 2022, 123: 191
24 Shamsolhodaei A, Oliveira J P, Schell N *et al*. *Intermetallics*[J], 2020, 116: 106 656
25 Santodonato L J, Zhang Y, Feygenson M *et al*. *Nature Communications*[J], 2015, 6(1): 5964
26 Jiang W T, Wang X H, Kang H J *et al*. *Journal of Alloys and Compounds*[J], 2022, 925: 166 767
27 Guo S, Liu C T. *Progress in Natural Science: Materials International*[J], 2011, 21(6): 433
28 Guo S, Ng C, Lu J *et al*. *Journal of Applied Physics*[J], 2011, 109(10): 103 505
29 Yurchenko N Y, Stepanov N D, Shaysultanov D G *et al*. *Materials Characterization*[J], 2016, 121: 125
30 Liu L Y, Zhang Y, Han J H *et al*. *Advanced Science*[J], 2021, 8(23): 2 100 870
31 Stepanov N D, Yurchenko N Y, Skibin D V *et al*. *Journal of Alloys and Compounds*[J], 2015, 652: 266
32 Yurchenko N Y, Stepanov N D, Zherebtsov S V *et al*. *Materials Science and Engineering A*[J], 2017, 704: 82
33 Huang T D, Wu S Y, Jiang H *et al*. *International Journal of Minerals*, *Metallurgy and Materials*[J], 2020, 27(10): 1318
34 Senkov O N, Wilks G B, Scott J M *et al*. *Intermetallics*[J], 2011, 19(5): 698
35 Senkov O N, Wilks G B, Miraclea D B *et al*. *Intermetallics*[J], 2010, 18(9): 1758
36 Xu Z Q, Ma Z L, Wang M *et al*. *Materials Science and Engineering A*[J], 2019, 755(7): 318
37 Huang T D, Jiang L, Zhang C L *et al*. *Science China Technological Sciences*[J], 2018, 61: 117

$Al_{0.5}Nb_{1.5}TiV_2Zr_{0.5}$难熔高熵合金组织和力学性能

蒋文韬[1]，王　晔[1]，姜　博[1]，王晓红[2]，马腾飞[2]，朱冬冬[2]
(1. 哈尔滨理工大学 材料科学与化学工程学院，黑龙江 哈尔滨 150040)
(2. 衢州学院 浙江省空气动力装备技术重点实验室，浙江 衢州 324000)

摘　要：采用真空电弧熔炼制备了$Al_{0.5}Nb_{1.5}TiV_2Zr_{0.5}$高熵合金，并研究了其微观组织、密度及力学性能。结果表明，$Al_{0.5}Nb_{1.5}TiV_2Zr_{0.5}$合金由为90.6%（体积分数）的体心立方相和9.4%（体积分数）的C14-Laves第二相组成。合金基体相富含Ti和V，第二相富含Al和Zr。合金的密度为6284 kg/m^3，维氏硬度为5197.9 MPa。合金的屈服强度随温度升高而降低，由室温下1082.9 MPa降低到1073 K下的645.0 MPa。压缩应变由室温下的27.20%降低到873 K下的14.94%，这与合金中原子间的相互作用力随温度升高而降低有关。在1073 K时合金应变超过50%，表现出良好的塑性而未发生断裂。压缩测试结果表明，合金韧脆转变温度在873~1073 K之间。

关键词：$Al_{0.5}Nb_{1.5}TiV_2Zr_{0.5}$；高熵合金；微观组织；硬度；压缩性能

作者简介：蒋文韬，男，1998年生，硕士，哈尔滨理工大学材料科学与化学工程学院，黑龙江 哈尔滨 150040，E-mail：littlee530@foxmail.com